Hindawi Publishing Corporation
Research Letters in Materials Science
Volume 2008, Article ID 737546, 5 pages
doi:10.1155/2008/737546

*Research Letter*

# TEM Nanostructural Study of Al-6Si-3Cu-$x$Mg Melt-Spun Ribbons

**Ismeli Alfonso López,[1] Cuauhtémoc Maldonado Zepeda,[2] Gonzalo González Reyes,[1] Ariosto Medina Flores,[2] and Juan Serrato Rodríguez[2]**

[1] *Instituto de Investigaciones en Materiales, Universidad Nacional Autónoma de México (UNAM) Circuito Exterior s/n, Cd. Universitaria, Del. Coyoacán CP 04510 México, DF, Mexico*
[2] *Instituto de Investigaciones Metalúrgicas, Universidad Michoacana de San Nicolás de Hidalgo, Morelia, CP 58000, Michoacán, Mexico*

Correspondence should be addressed to Ismeli Alfonso López, ialfonso@iim.unam.mx

Received 29 February 2008; Accepted 10 April 2008

Recommended by Martin Crimp

Three quaternary Al-6Si-3Cu-$x$Mg ($x$ = 0.59, 3.80, and 6.78 wt.%) alloys were produced by melt-spun and characterized using X-ray diffractometry (XRD), transmission electron microscopy (TEM), and microhardness techniques. Obtained second phases were $Al_2Cu(\theta)$ for the alloy with 0.59% Mg and $Al_5Cu_2Mg_8Si_6$ (Q) for the alloys with 3.80 and 6.78% Mg. These phases are present as 30–50 nm or as 5–10 nm nanoparticles. Alloying elements content in solid solution increased, mainly for Si and Mg. The high alloying elements content in solid solution and the small $\alpha$-Al cell size for melt-spun alloys leads to microhardness values about 2 times higher than those of ingot counterparts. The microhardness increase for melt-spun alloys with 3.80 and 6.78% Mg depends on Mg content in solid solution.



## 1. INTRODUCTION

Among the aluminum alloys, the 319 is one of the most widely used Al-Si-Cu-Mg alloys in the automotive industry. This alloy presents Si contents from 5.5 to 6.5 and Cu in the range from 3.0 to 4.0 wt% [1]. The cast structure for Al-Si-Cu-Mg alloys includes $\alpha$-Al, Si eutectic particles, $Mg_2Si$, $Al_2Cu$, $Al_5Cu_2Mg_8Si_6$, and other complex intermetallics [1, 2]. Applying a rapid solidification process (RSP) as melt-spinning, it is possible to avoid or minimize second phase formation and obtain a supersaturated solid solution. Melt-spun produces metastable crystalline, nanocrystalline, and amorphous phases, with improved mechanical properties [3].

There was a previous work about the characterization of Al-Si-Cu alloys [4] obtained by melt spun, remarking the solid solubility extension of Si in $\alpha$-Al. However, the effects of RSP on structure and properties when Mg is added have not been reported in the literature. Mechanical properties improvement for these alloys has been related to nanocrystalline and amorphous phase formation. In this work, nanostructure and mechanical properties for the experimental 319 alloy are dealt with by examining melt-spun ribbons with three different Mg concentrations, analyzing the effect of Mg on nanostructure and on the quantity of alloying elements in solid solution, and their relationship with the mechanical properties.

## 2. EXPERIMENTAL

The master alloy was an A 356 alloy ingot with Al-8.5Si-0.3Mg (wt%), adding pure Cu and Mg. Castings were carried out in graphite crucibles using an induction furnace under a controlled Ar atmosphere. Ingots were then remolten in a quartz tube and ejected through a 0.5-mm diameter aperture on to the surface of a 200-mm in diameter polished copper wheel rotating at 30 meters per second$^{-1}$. The ribbons were 20–60 $\mu$m in thickness. Table 1 shows the alloys chemical composition.

Experimental alloys were characterized using XRD, TEM/STEM, and microhardness techniques. XRD measurements were carried out in a Siemens 400 X-ray diffractometer

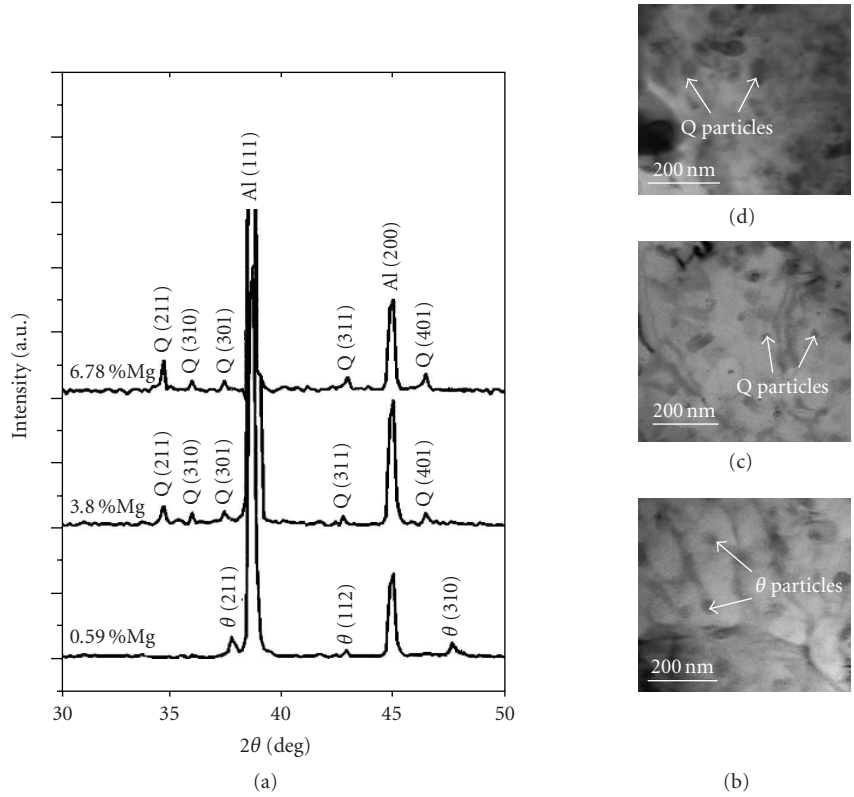


Figure 1: XRD profiles of the ribbons for the alloys with different Mg contents (a) and bright field transmission electron micrographs of the as-melt-spun ribbons for the alloys with: (b) 0.59% Mg, (c) 3.80% Mg, and (d) 6.78% Mg. Diffraction peaks belonging to $\theta$ and Q are correlated to the presence of arrowed nanoparticles.

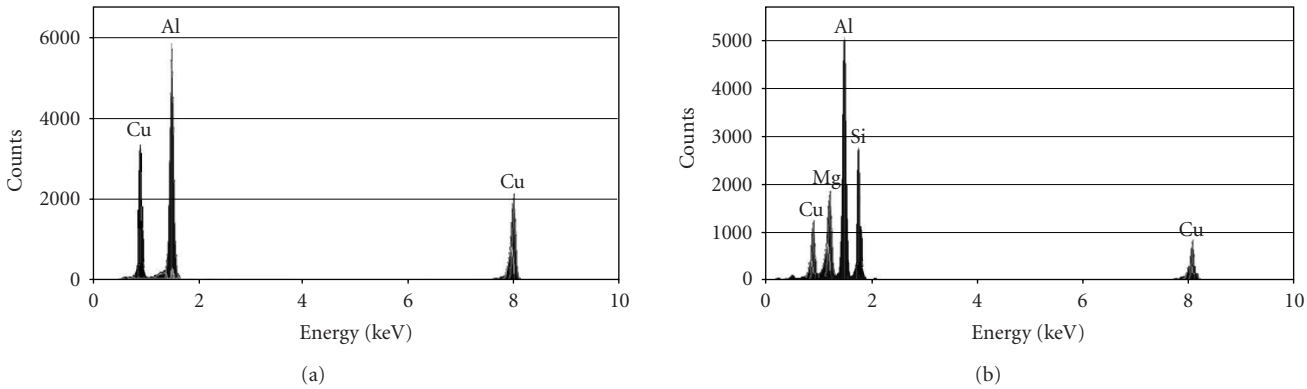


Figure 2: EDS analysis obtained from the second phases: (a) for ribbons with 0.59% Mg and (b) for ribbons with 3.80% Mg.

using CuK$\alpha$ radiation at 30 kV and 25 mA. TEM/STEM and HRTEM investigations were conducted using a FEG-Philips Tecnai F20 scanning/transmission electron microscope operated at 200 kV, equipped with an energy dispersive spectrometry (EDS) with internal software for qualitative, semiquantitative and quantitative chemical analysis. In order to obtain repetitive and accurate results for each specimen 10 spectra were collected and averaged. Each spectrum was collected in only 10 seconds to avoid the electron beam to drift over the sample resulting in reduced statistics. Specimens for TEM were prepared by dimpling using a Gatan 656 Dimple Grinder followed by Argon ions milling using a Gatan 691 Precision Ion Polishing System (PIPS). HRTEM micrographs were processed using Digital Micrograph(TM) 3.7.0 (Gatan). Microhardness measurements were made with a Vickers diamond indenter in a Leitz Wetzlar microhardness tester employing a load of 25 g for 15 seconds. Statistical treatment criteria were used to get repetitive and accurate results.

## 3. RESULTS AND DISCUSSION

In ternary Al systems, previous works report ample solid solubility of alloying elements in $\alpha$-Al matrix and minimum second phase formation as result of rapid solidification [3, 4].

Table 1: Average chemical composition (in wt%) of the experimental alloys.

| Alloy code | Si | Cu | Mg | Fe | Mn | Zn | Ti | Al |
|---|---|---|---|---|---|---|---|---|
| AM01 | 6.40 | 3.02 | 0.59 | 0.34 | 0.09 | 0.04 | 0.14 | Balance |
| AM03 | 6.31 | 3.03 | 3.80 | 0.32 | 0.08 | 0.03 | 0.13 | Balance |
| AM06 | 5.84 | 2.95 | 6.78 | 0.31 | 0.07 | 0.03 | 0.12 | Balance |

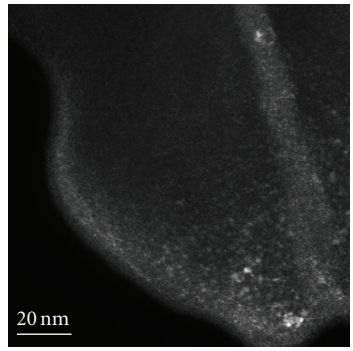


Figure 3: TEM-dark field micrograph showing the presence of nanoparticles for ribbons with 0.59% Mg.

These effects are also expected for quaternary Al-Si-Cu-Mg alloys. XRD evidence in Figure 1(a) suggests limited solid solution for the melt-spun ribbons. Besides diffraction peaks corresponding to $\alpha$-Al, diffraction peaks associated to $\theta$ ($Al_2Cu$) were visible for ribbons with 0.59% Mg, while peaks associated to Q ($Al_5Cu_2Mg_8Si_6$) were observed for ribbons with 3.80 and 6.78%. The intensity of Q peaks increased for the alloy with higher Mg content. This suggests the content of free Q phase increases, an expected result because of the high quantity of Mg in the alloy with 6.78% Mg. Despite the limited solubility, XRD analysis shows that melt-spun reduced formation of second phases. No evidence of diffraction peaks belonging to Si, Al-Si eutectic, or other complex intermetallic phases (present in conventionally cast alloys for this quaternary system [5]) were observed from melt-spun XRD spectra. TEM techniques were applied to correlate XRD diffraction peaks with microstructure and to further study second phases. Bright field transmission electron micrograph of the ribbons shown in Figures 1(b)–1(d) revealed the presence of 30–50 nm second phase irregular particles (arrowed). One can see the contrast in the images, revealing the existence of other phases besides $\alpha$-Al matrix. Diffraction peaks belonging to $\theta$ and Q (see Figure 1(a)) are correlated to the presence of these nanoparticles. The presence of these second phases also corroborates the limited solid solubility revealed using XRD. The quaternary Q phase is present as an equilibrium phase at most of the compositions in these quaternary systems. In our study, the distinction between the Q stable phase and its precursors (Q′, QC, and QP, all metastable phases) was made taken into account XRD results. These precursors are coherent phases [6, 7]. Nevertheless, a large overlapping between different Qs phases exists and then the presence of metastable or precursor phases can always be possible.

Table 2: Average atomic percent of alloying elements in the supersaturated solid solution for the alloys obtained using rapid solidification and conventional casting.

| Alloy code | Ribbons | | | Ingots | | |
|---|---|---|---|---|---|---|
| | Si | Mg | Cu | Si | Mg | Cu |
| AM01 | 9.0 | 0.2 | 1.3 | 1.4 | 0.1 | 0.3 |
| AM03 | 6.6 | 2.5 | 1.0 | 0.7 | 0.1 | 0.7 |
| AM06 | 4.4 | 6.7 | 0.9 | 0.3 | 0.1 | 1.5 |

Table 3: Microhardness values for ribbons and ingots.

| Mg content (wt%) | Microhardness (Vickers hardness no.) | |
|---|---|---|
| | Ribbons | Ingots |
| 0.59 | 164.3 ± 4.2 | 86.4 ± 3.4 |
| 3.80 | 183.4 ± 4.1 | 88.2 ± 2.6 |
| 6.78 | 190.6 ± 5.2 | 87.7 ± 2.1 |

Relationship between diffraction peaks and particles commented above is based on EDS studies of regions with a darker contrast observed in Figures 1(b)–1(d). EDS analysis carried out in particles of alloy with 0.59% Mg, as depicted in Figure 2(a), shows Al and Cu signals. While analysis for particles in the alloy with 3.80% Mg, as seen in Figure 2(b), shows Al, Si, Cu, and Mg signals. For the alloys with 0.59% Mg an Al:Cu ratio close to 2:1 confirms that regions with a darker contrast observed in Figure 1(b) correspond to $\theta$. For the alloys with 3.80 and 6.78% Mg Al:Cu:Mg:Si ratios indicate that regions with a darker contrast observed in Figures 1(c) and 1(d) correspond to Q. These compositions are consistent with XRD results.

Despite limited solid solubility, RSP led to high concentration of alloying elements in the supersaturated solid solution ($\alpha$-Al), as seen in Table 2. EDS analysis was used to get comparable results. Alloying elements concentration in solid solution was increased for melt-spun ribbons, mainly for Si and Mg. These high alloying elements in solid solution are not possible using conventional casting even after quenching.

An exhaustive analysis of the ribbons showed the presence of well spread approximately 5 nm nanoparticles for all the melt-spun alloys. Dark field technique was advantageously used to detect low-contrast nanoparticles. A TEM dark field image of ribbons with 0.59% Mg is observed in Figure 3. Nanoparticles can be observed. This image was obtained from the most intense halo ring of the diffraction pattern.

We further tried to clarify the details of nanoparticles by HRTEM. Figure 4(a) shows HRTEM micrograph of ribbons

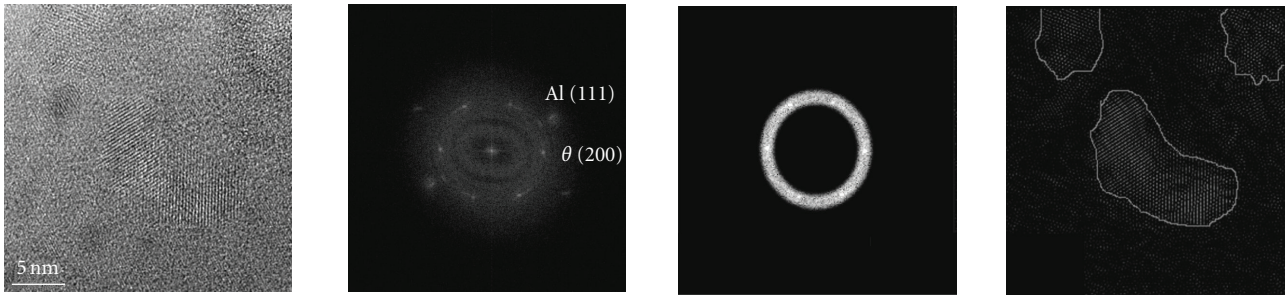


Figure 4: (a) HRTEM micrograph of the alloy with 0.59% Mg showing $\theta$ nanocrystallites; (b) FFT of the image; (c) frequencies corresponding to $\theta$ to produce the IFFT image and (d) IFFT image isolating the $\theta$ nanoparticles.

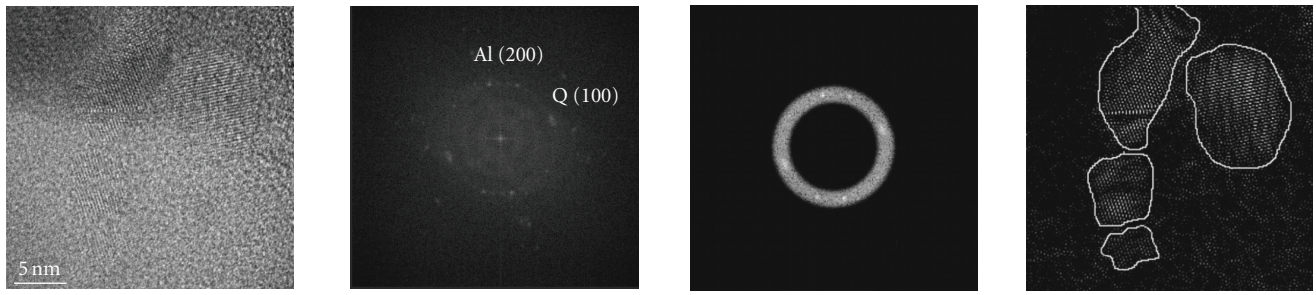


Figure 5: (a) HRTEM image of the melt-spun ribbons with 3.80% Mg showing Q nanocrystallites; (b) FFT of the image; (c) frequencies corresponding to Q to produce the IFFT image and (d) IFFT image isolating the Q nanoparticles.

with 0.59% Mg. As noted, nanocrystallites are present in the $\alpha$-Al matrix. The fast Fourier transform (FFT) depicted in Figure 4(b) shows the frequencies attributed to crystallites of $\theta$ and the $\alpha$-Al phase. The composition of the nanosized particles was determined using nanobeam EDS (3 nm in diameter spot size), indicating that it is close to $Al_2Cu$ ($\theta$). To study the morphology of the nanosized particles inverse-FFT (IFFT) using $\theta$ frequencies were obtained (see Figures 4(c), 4(d)). As observed, nanoparticles have irregular shapes. The filtered image for the (200) plane showed the interplanar distance matching to $Al_2Cu$ (3.04 Å).

The increase in Mg content (alloy with 3.80% Mg) also leads to formation of nanoparticles distributed in a similar fashion as those of 0.59% Mg alloy. The nanobeam EDS analysis of these nanoparticles revealed the presence of elements with ratios near to the stechiometric ratios for Q phase ($Al_5Cu_2Mg_8Si_6$). Q phase was originated by the increase in Mg content and is also observed for the alloy with 6.78% Mg. Figure 5(a) shows an HRTEM micrograph for ribbons with 3.80% Mg. Q phase nanocrystallites can be observed. The FFT depicted in Figures 5(b), 5(c) shows the frequencies attributed to crystallites of Q phase. IFFT image obtained for Q frequencies revealed the irregular shape of nanoparticles (see Figure 5(d)). The interplanar distance (3.16 Å) corresponding to Q(200) plane corroborates EDS results.

Table 3 shows microhardness values for ribbons and ingots. Ribbons hardness values are about 2 times higher than those of ingots with the same composition. Hardening mechanisms of Al alloys can be described by several contributing factors: Hall-Petch hardening from the $\alpha$-Al cell size, solid solution hardening of $\alpha$-Al matrix, and particle size (according to Orowan hardening). Wang et al. [8] found that for melt-spun alloys, microhardness is mainly governed by a combination of Hall-Petch hardening from the small $\alpha$-Al cell size and solid solution hardening of the $\alpha$-Al matrix, whereas the Orowan hardening from the nanoparticles is negligible. The increase in microhardness for the ribbons with 3.80 and 6.78% Mg could be related to the presence of a higher Mg content in solid solution, besides the increase of the volume fraction of Q phase.

## 4. CONCLUSIONS

From XRD and TEM analysis, it can be concluded that using melt-spun second phase formation was minimized and alloying elements concentration in solid solution was increased. Second phases composition depends on Mg content: $Al_2Cu$ for the alloy with 0.59% Mg and $Al_5Cu_2Mg_8Si_6$ for the alloys with 3.80 and 6.78% Mg. These phases are present as 30–50 nm nanoparticles. HRTEM studies also concluded the presence of these phases as 5–10 nm nanoparticles.

Microhardness values of melt-spun ribbons are between 160 and 190 VHN, about 2 times higher than those of conventionally cast alloys with the same composition. Hardness improvement is originated from the high alloying elements concentration in the supersaturated solid solution and from nanostructure originated for the small $\alpha$-Al cell size, besides the presence of nanoparticles.

## ACKNOWLEDGMENTS

The authors are thankful to F. Solorio and R. D. Cervantes from IIM-UMSNH and G. Lara from IIM-UNAM, México, for technical support.

## REFERENCES

[1] P. Ouellet and S. H. Samuel, "Effect of Mg on the aging behaviour of Al-Si-Cu 319 type aluminium casting alloys," *Journal of Materials Science*, vol. 34, no. 19, pp. 4671–4697, 1999.

[2] Z. Li, A. M. Samuel, F. H. Samuel, C. Ravindran, and S. Valtierra, "Effect of alloying elements on the segregation and dissolution of $CuAl_2$ phase in Al-Si-Cu 319 alloys," *Journal of Materials Science*, vol. 38, no. 6, pp. 1203–1218, 2003.

[3] H. H. Liebermann, "Rapidly solidified alloys made by chill block melt-spinning processes," *Journal of Crystal Growth*, vol. 70, no. 1-2, pp. 497–506, 1984.

[4] M. L. Öveçoğlu, N. Ünlü, N. Eruslu, and A. Genç, "Characterization investigations of a melt-spun ternary Al-8Si-5.1Cu (in wt.%) alloy," *Materials Letters*, vol. 57, no. 21, pp. 3296–3301, 2003.

[5] I. Alfonso, C. Maldonado, G. Gonzalez, and A. Bedolla, "Effect of Mg content and solution treatment on the microstructure of Al-Si-Cu-Mg alloys," *Journal of Materials Science*, vol. 41, no. 7, pp. 1945–1952, 2006.

[6] C. Cayron and P. A. Buffat, "Transmission electron microscopy study of the $\beta'$ phase (Al-Mg-Si alloys) and QC phase (Al-Cu-Mg-Si alloys): ordering mechanism and crystallographic structure," *Acta Materialia*, vol. 48, no. 10, pp. 2639–2653, 2000.

[7] D. J. Chakrabarti and D. E. Laughlin, "Phase relations and precipitation in Al-Mg-Si alloys with Cu additions," *Progress in Materials Science*, vol. 49, no. 3-4, pp. 389–410, 2004.

[8] Y. Wang, Z. Zhang, W. Wang, and X. Bian, "Microstructural evolution and microhardness of a melt-spun Al-5Ti-1B alloy during annealing," *Materials Science and Engineering A*, vol. 366, no. 1, pp. 17–24, 2004.